Supplementary Information

Solvent-Accelerated Photoreduction of Hg(II) Dihalides: Uncovering Solvent-Governed and Light-Triggered Mercury Chemistry

Donghwan Im[a,b†], Alekos Segalina[a,b†], and Hyotcherl Ihee[a,b]*

[a] Department of Chemistry, Korea Advanced Institute of Science and Technology (KAIST), Daejeon 34141, Republic of Korea

[b] Center for Advanced Reaction Dynamics (CARD), Institute for Basic Science (IBS), Daejeon 34141, Republic of Korea

† These authors contributed equally to this work.

*Hyotcherl Ihee: E-mail: hyotcherl.ihee@kaist.ac.kr

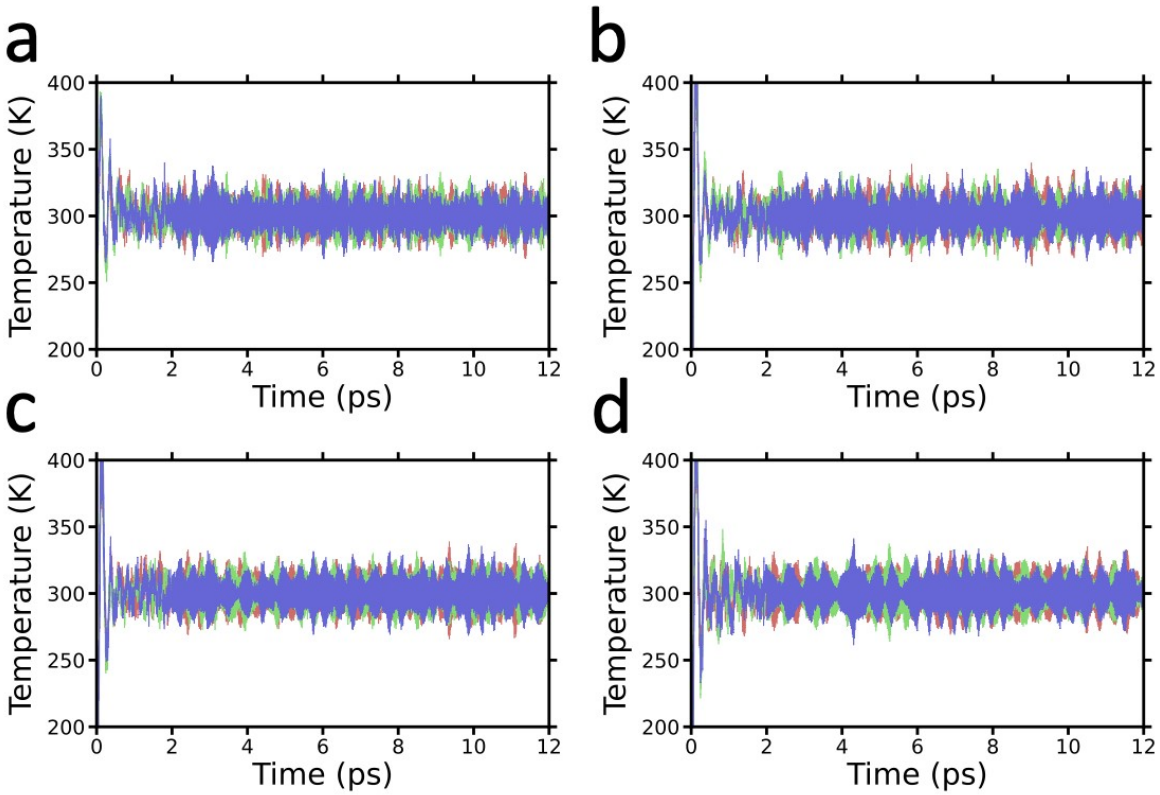

Fig. S1 Temperature fluctuations of HgI_2 in (a) water, (b) MeOH, (c) DMSO, and (d) pyridine during AIMD simulations. Each of the three colors represents the behavior of an independent trajectory.

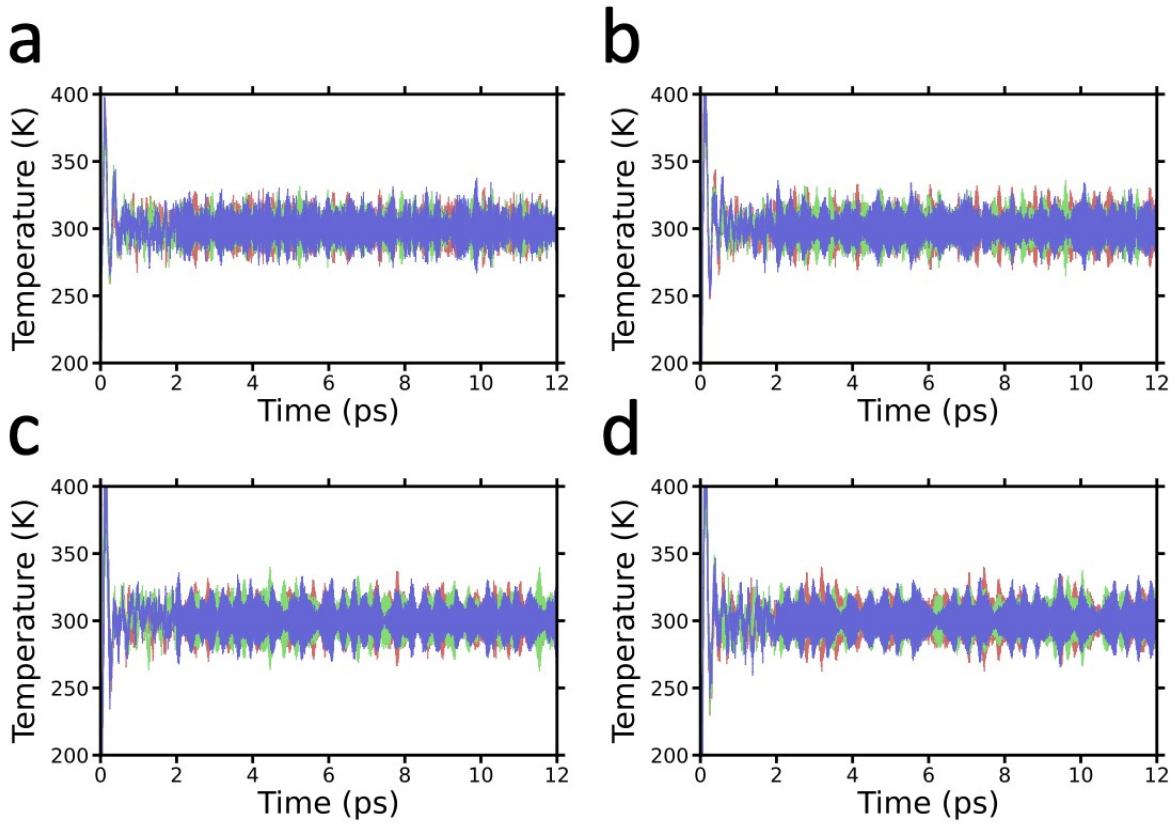

Fig. S2 Temperature fluctuations of $HgBr_2$ in (a) water, (b) MeOH, (c) DMSO, and (d) pyridine during AIMD simulations. Each of the three colors represents the behavior of an independent trajectory.

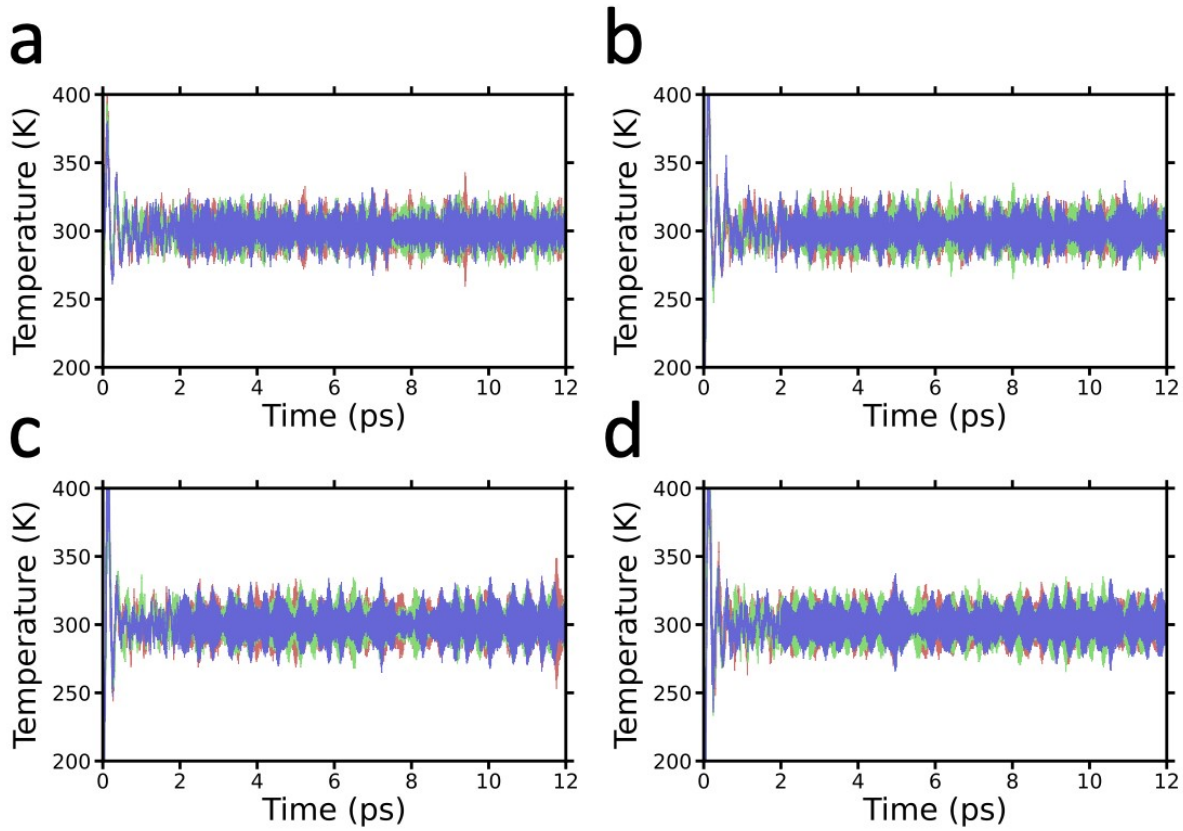

Fig. S3 Temperature fluctuations of $HgCl_2$ in (a) water, (b) MeOH, (c) DMSO, and (d) pyridine during AIMD simulations. Each of the three colors represents the behavior of an independent trajectory.

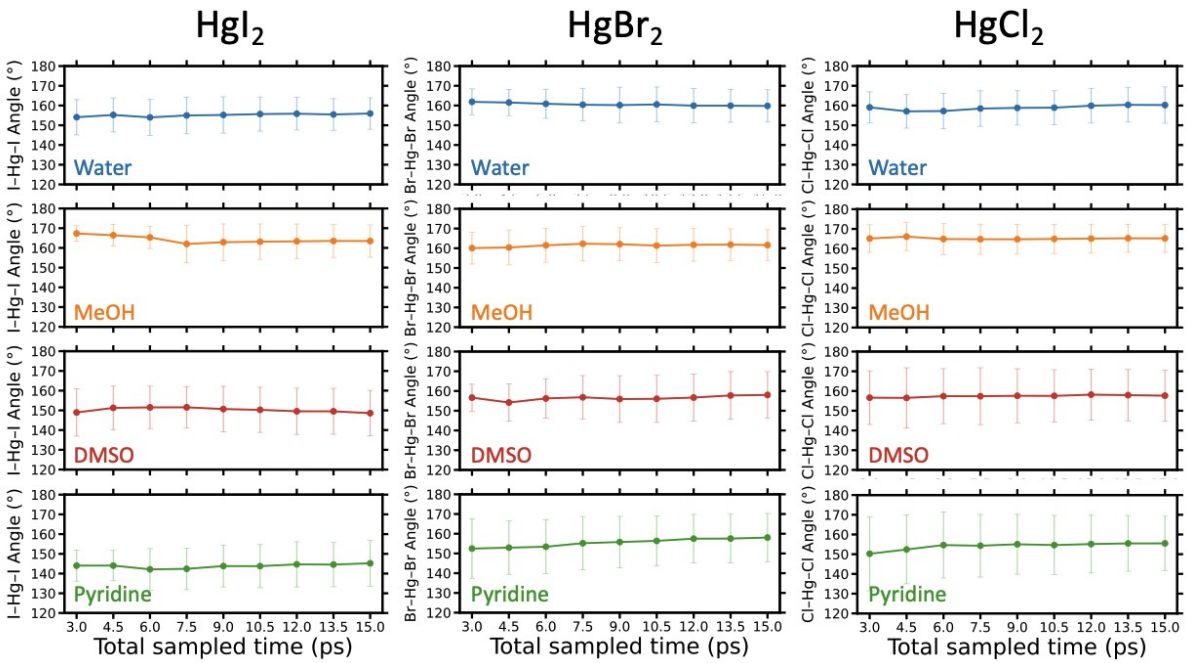

Fig. S4 Averaged X–Hg–X (X = I, Br, Cl) angles and associated standard deviations derived from AIMD simulations, performed in water (blue), MeOH (orange), DMSO (red), and pyridine (green). Statistical averages were evaluated as a function of total length of the sampled trajectories. (three independent 15 ps trajectories per system; analysis performed over the last 5 ps of each trajectory, yielding 15 ps of total analyzed sampling).

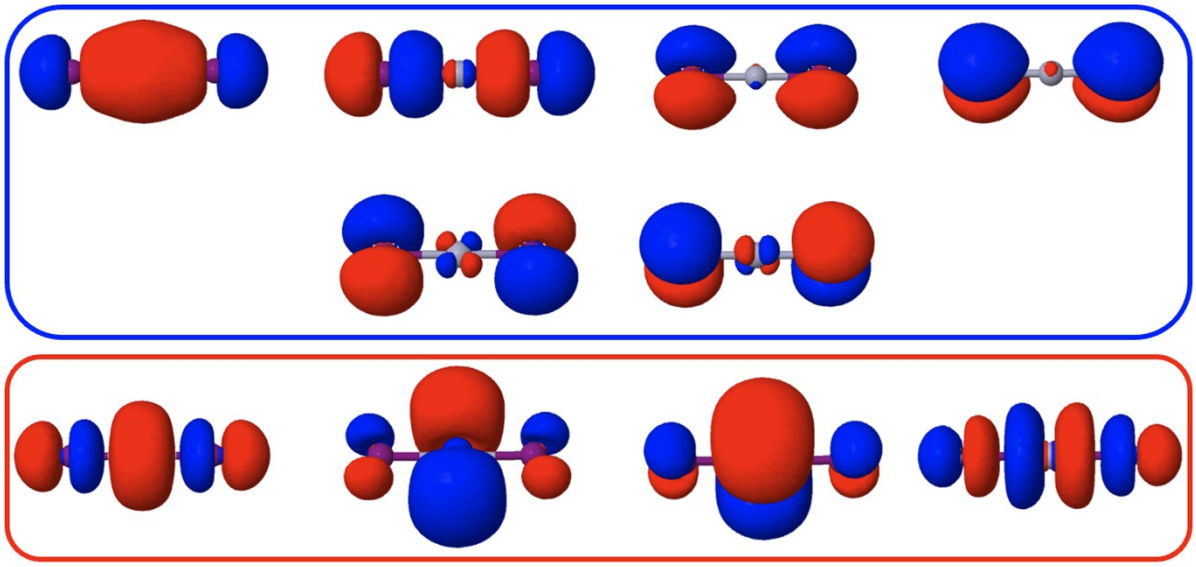

Fig. S5 Selected active space (12e, 10o) for the HgX_2 molecules. The active space includes the σ, σ*, and nonbonding orbitals of the halogen and mercury atoms, consistent with a previous report.[S1] Orbitals with predominantly occupied character in the reference Hartree–Fock determinant (i.e., the single-configuration reference used to define the CASSCF active space) are enclosed in blue boxes, while those with mainly virtual character are enclosed in red boxes.

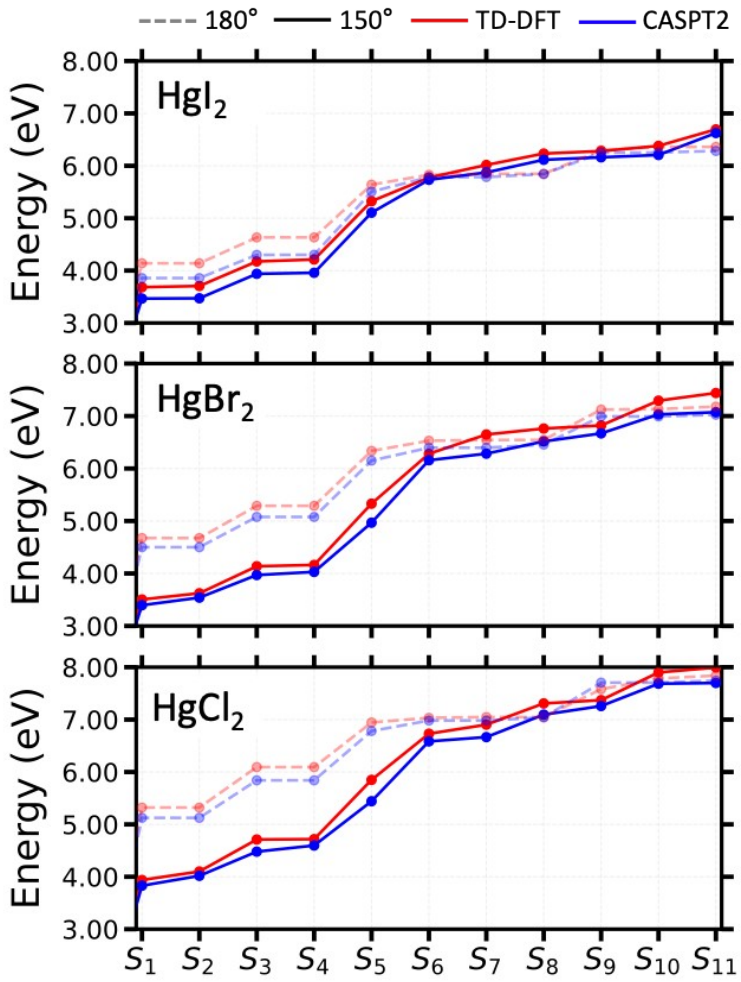

Fig. S6 Comparison of excited-state energy levels calculated using TD-DFT (red) and CASPT2 (blue) for linear (180°, dotted lines) and bent (150°, solid lines) X–Hg–X geometries, showing similar trends for the two methods in both configurations.

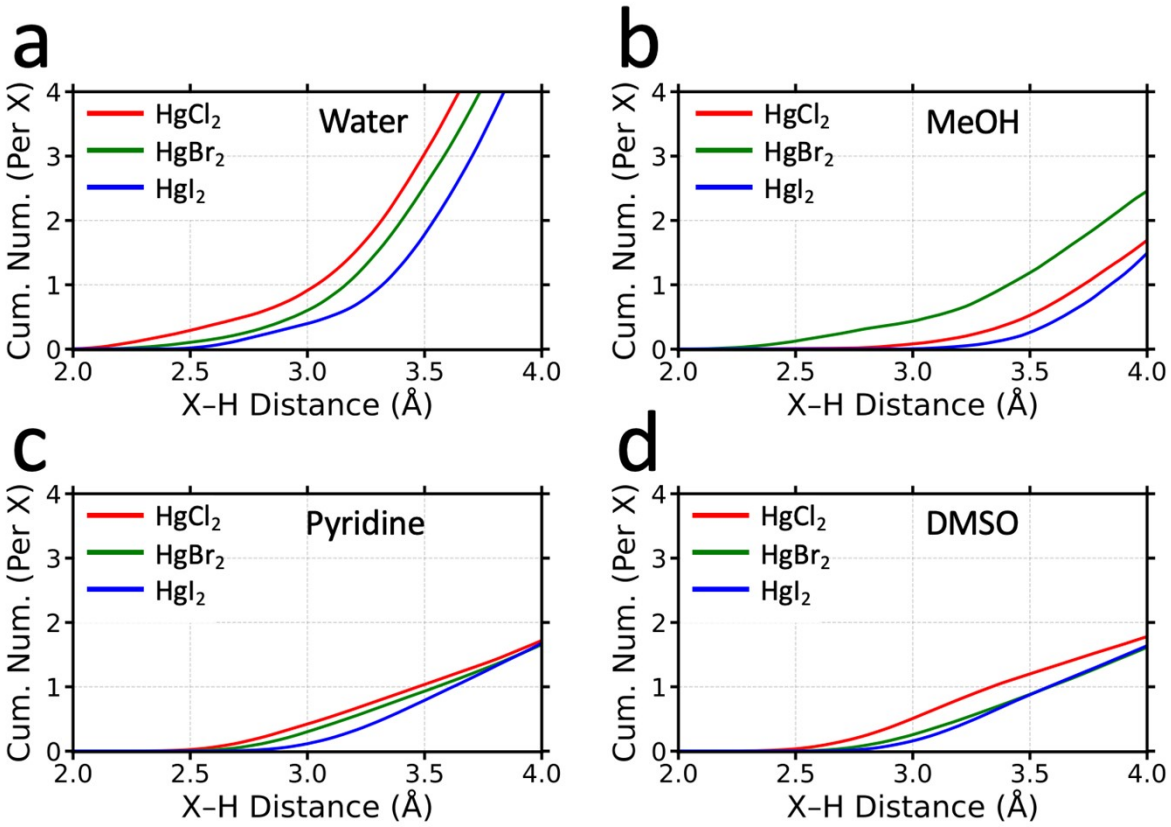

Fig. S7 Calculated cumulative number density functions (CDFs) between halogen (X) atoms and solvent hydrogens, obtained from AIMD trajectories of HgX_2 molecules in (a) water, (b) MeOH, (c) pyridine and (d) DMSO. For MeOH, CDFs were calculated between the hydroxyl hydrogen and the halogen atoms.

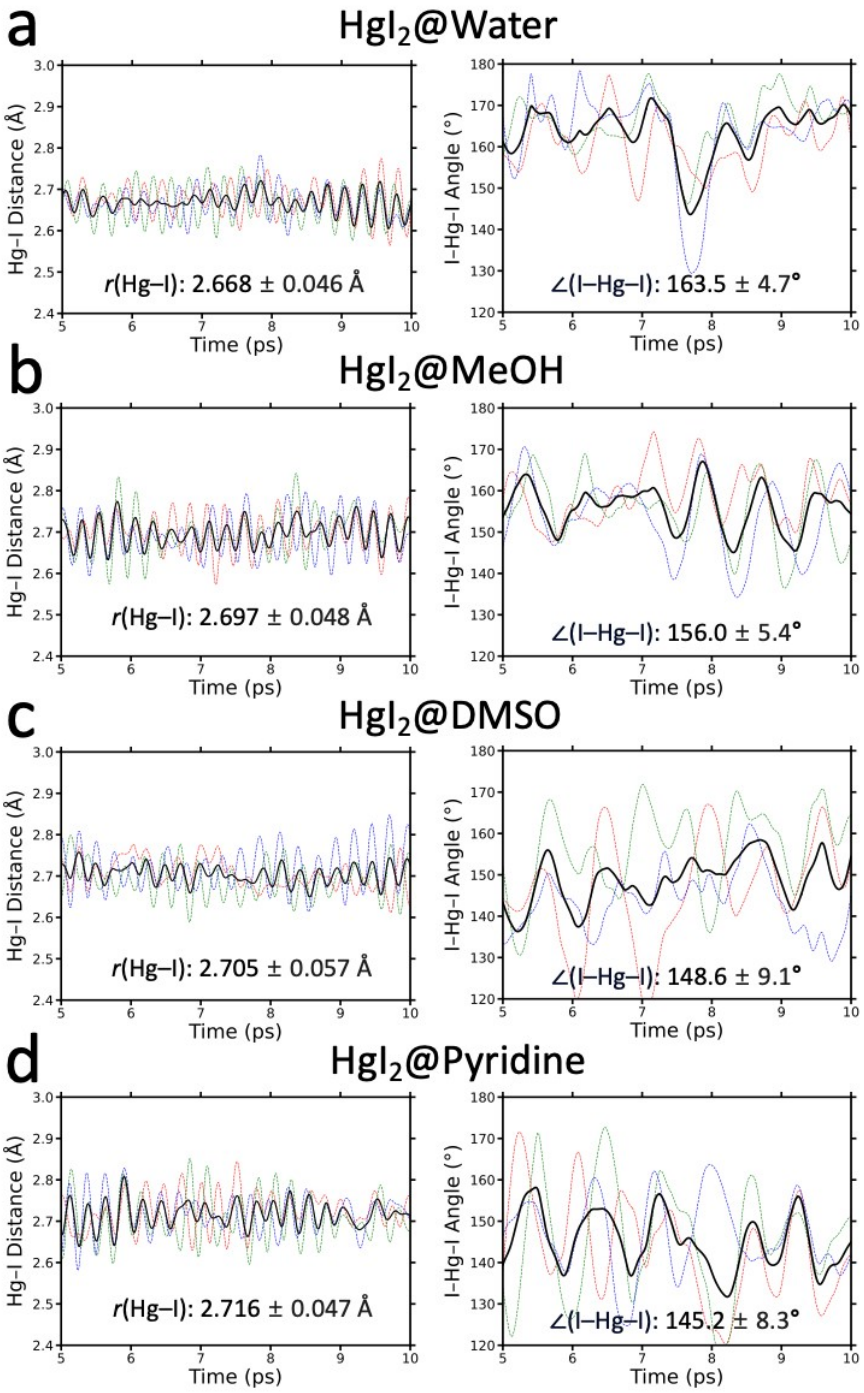

Fig. S8 Hg–I distances and I–Hg–I angle of HgI_2, calculated in four different solvents: (a) water, (b) MeOH, (c) DMSO, and (d) pyridine. The solid black line represents averaged values across three independent AIMD trajectories, while the colored dotted lines indicate values from individual trajectories. In each panel, the averaged structural parameter is reported along with its first standard deviation to reflect the extent of structural fluctuations. The geometric trend of each independent trajectory is illustrated using a different color.

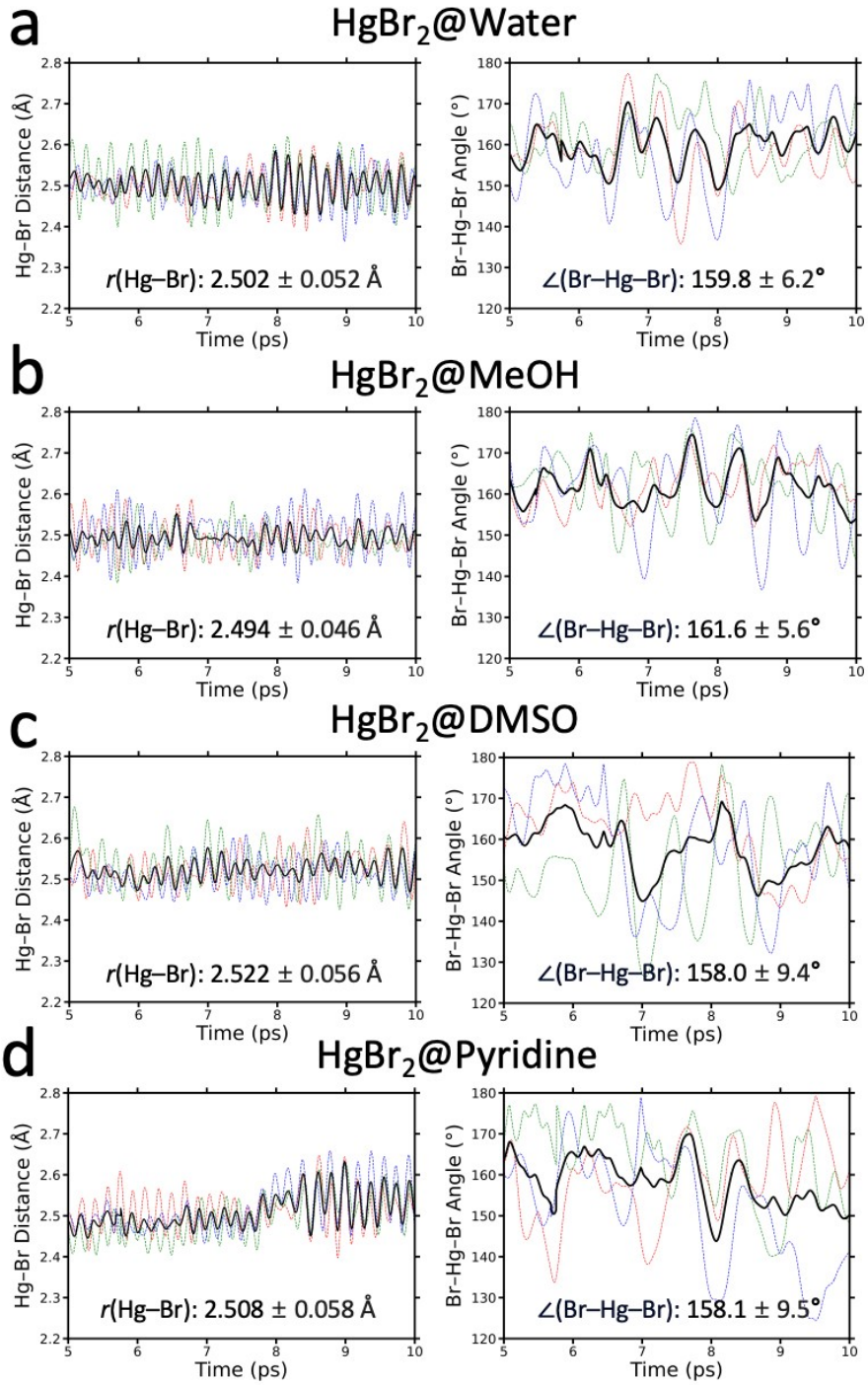

Fig. S9 Hg–Br distances and Br–Hg–Br angle of $HgBr_2$, calculated in four different solvents: (a) water, (b) MeOH, (c) DMSO, and (d) pyridine. The geometric trend of each independent trajectory is illustrated using a different color.

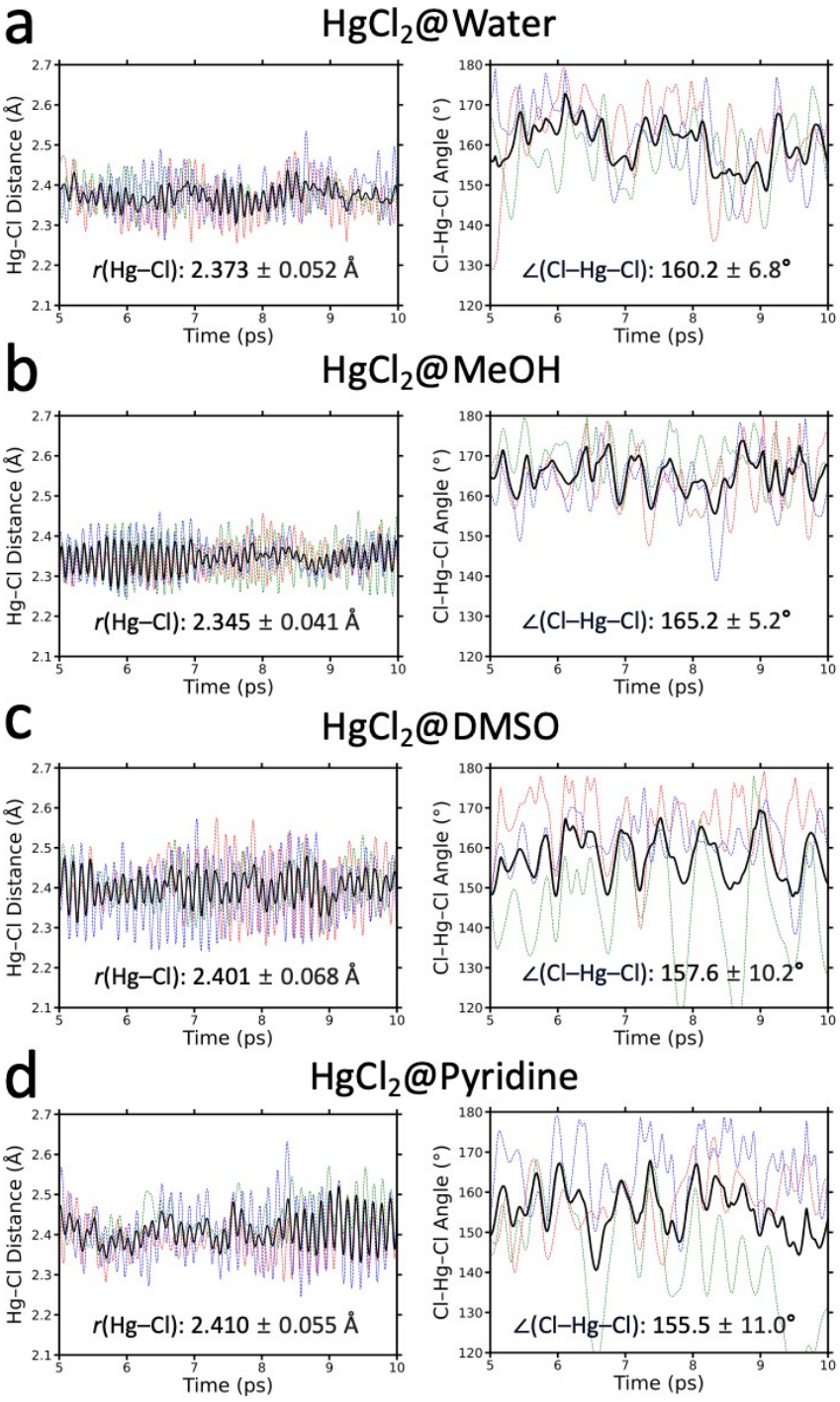

Fig. S10 Hg–Cl distances and Cl–Hg–Cl angle of $HgCl_2$, calculated in four different solvents: (a) water, (b) MeOH, (c) DMSO, and (d) pyridine. The geometric trend of each independent trajectory is illustrated using a different color.

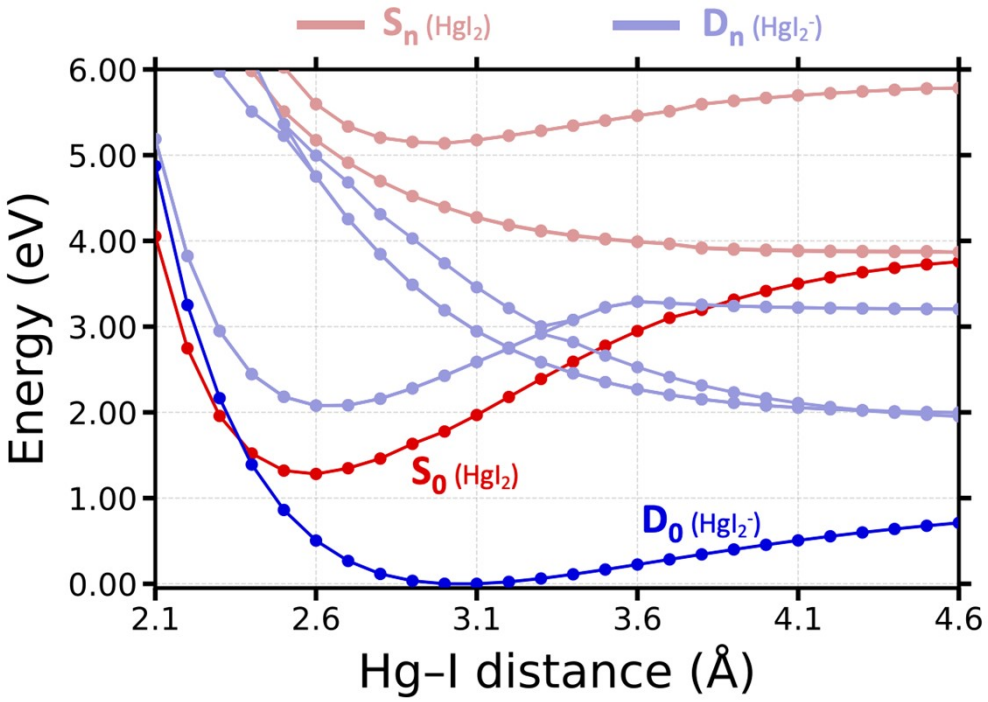

Fig. S11 Potential energy curve (PECs) of HgI_2 and HgI_2^- along the Hg–I distances. Singlet states of HgI_2 are shown in red, and doublet states of HgI_2^- are shown in blue.

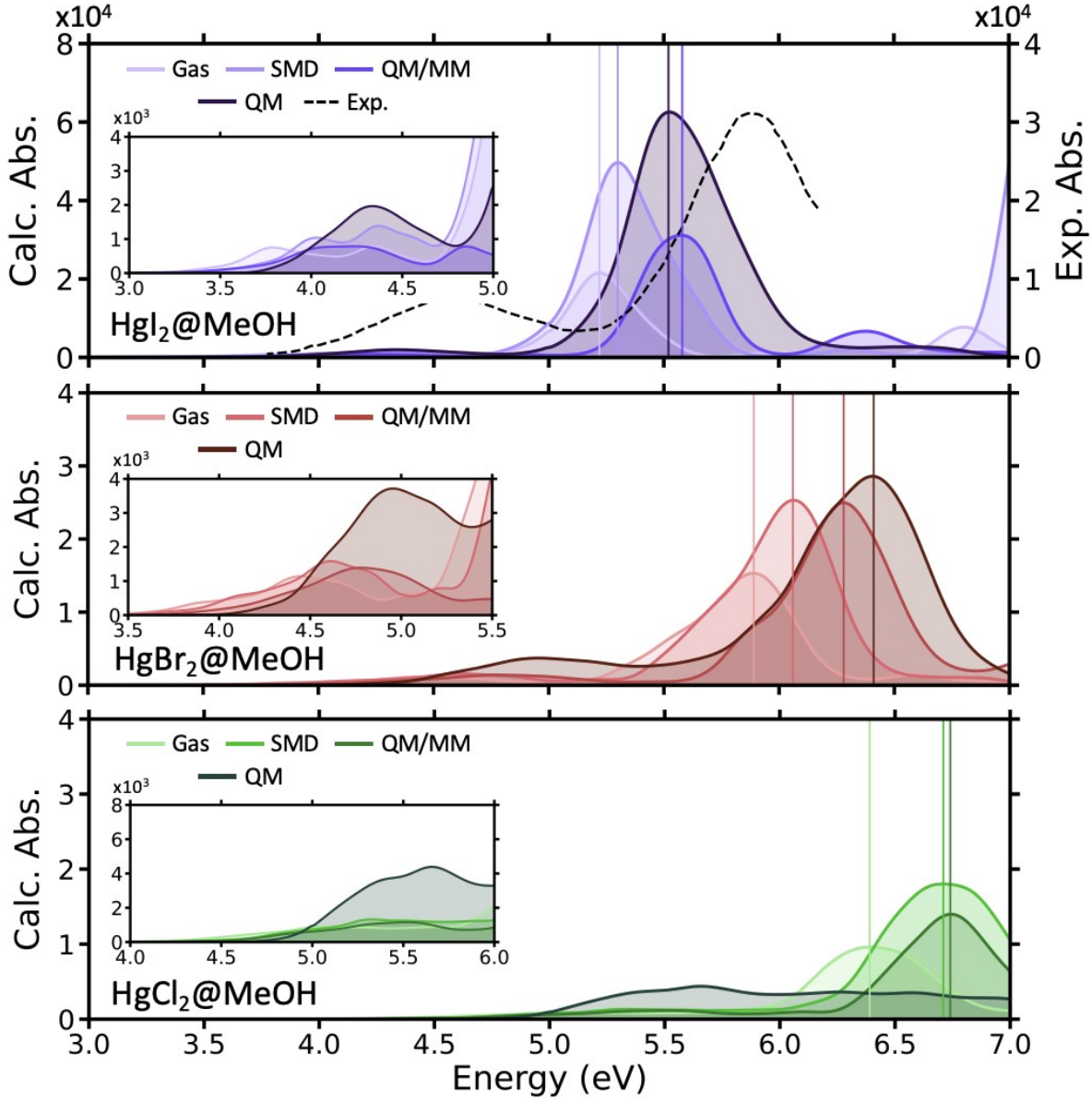

Fig. S12 Calculated absorption spectra of HgI_2 (top), $HgBr_2$ (middle), and $HgCl_2$ (bottom) in MeOH, based on 300 snapshots taken from AIMD simulation. This figure for MeOH is the counterpart to Figure 4, which depicts the results for water. Spectra were calculated using three different treatments of the solvent: (i) gas-phase spectra computed from the same AIMD geometries without solvent (Gas); (ii) spectra obtained with the implicit SMD solvent model (SMD); (iii) spectra calculated using the QM/MM approach, with the solvent described by a force field (QM/MM) and (iv) spectra with 30 explicit MeOH molecules treated quantum mechanically, combined with the implicit SMD solvent model (QM). The inset shows a magnified view of the first absorption peak of the calculated absorption spectrum. For comparison, the experimental absorption spectra of HgI_2 measured in MeOH is shown as dotted lines, taken from ref S1.

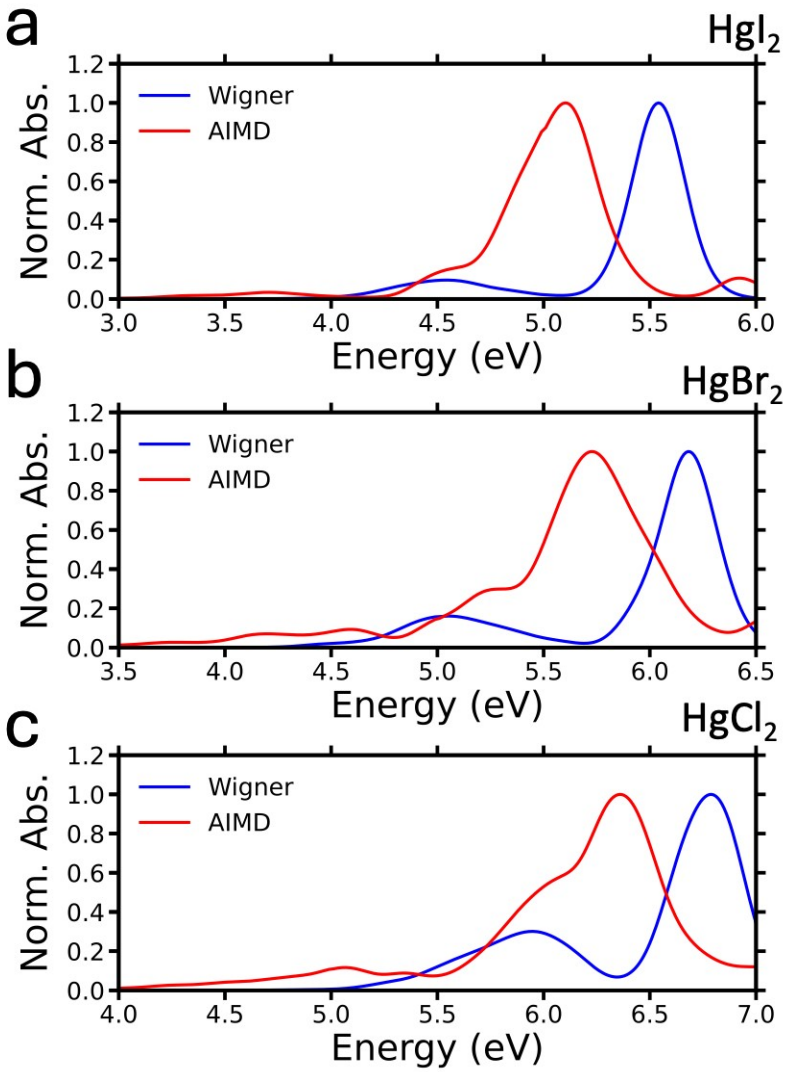

Fig. S13 Calculated gas-phase absorption spectra of (a) HgI_2, (b) $HgBr_2$, and (c) $HgCl_2$, using two sets of structures: one obtained from Wigner sampling of the linear gas-phase geometry (shown in blue), and the other from nuclear configurations extracted from AIMD simulations (shown in red).

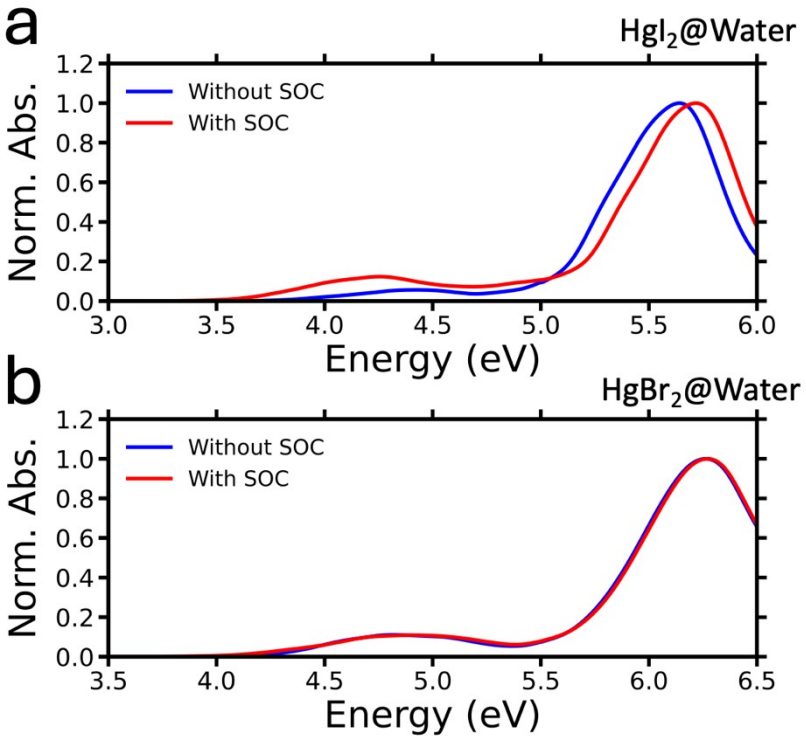

Fig. S14 Calculated absorption spectra of (a) HgI_2 and (b) $HgBr_2$ in water, comparing results without spin–orbit coupling (blue) and with spin–orbit coupling (red).

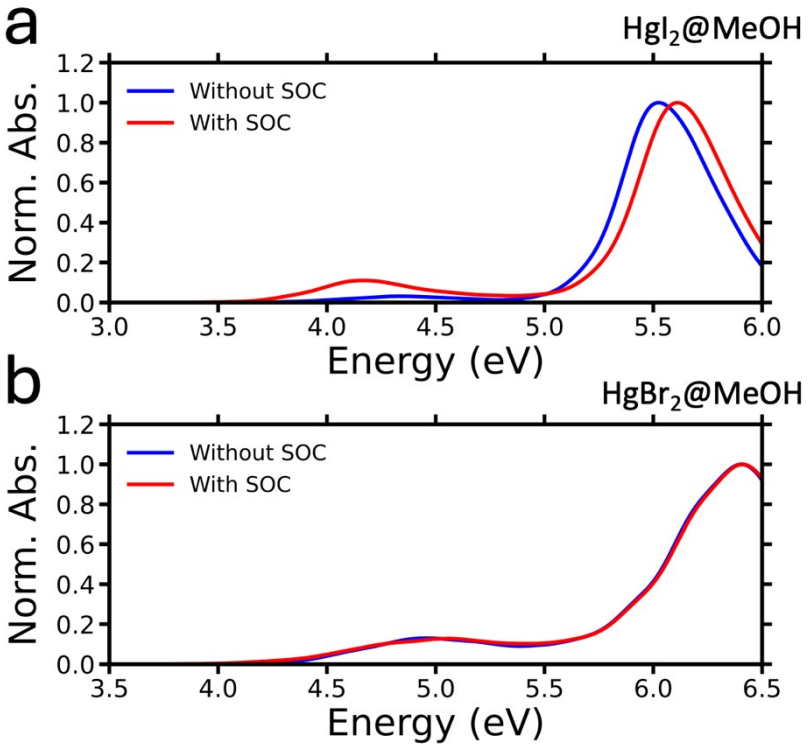

Fig. S15 Calculated absorption spectra of (a) HgI_2 and (b) $HgBr_2$ in MeOH, comparing results without consideration of spin–orbit coupling (blue) and with spin–orbit coupling (red).

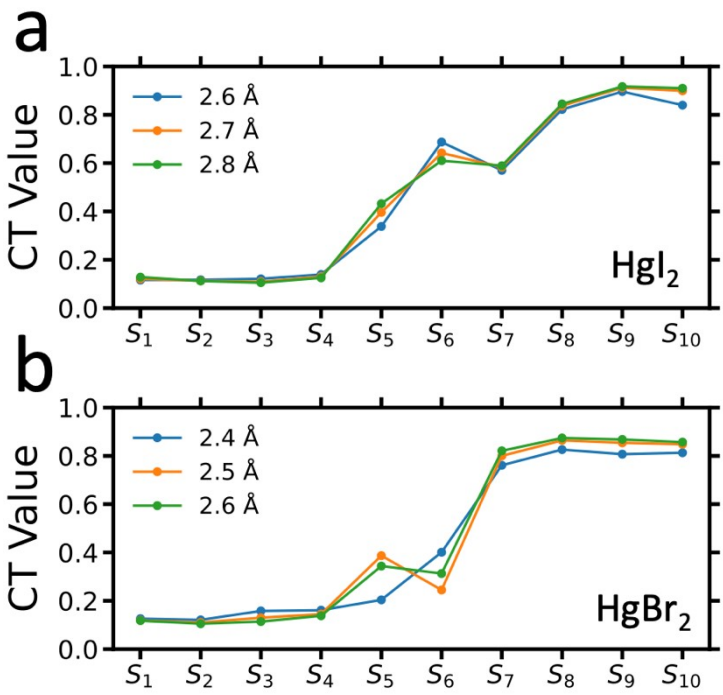

Fig. S16 Charge-transfer (CT) values corresponding to the solvent-to-solute CT character, obtained from one-particle transition density matrix (1-TDM) analysis for HgX_2 (X = I, Br), computed at different symmetric Hg–X bond lengths. The two Hg–X bonds were constrained to be equal. Variations in the bond length result in only minor changes in the CT values, indicating a weak dependence of the solvent-to-solute CT character on Hg–X bond elongation.

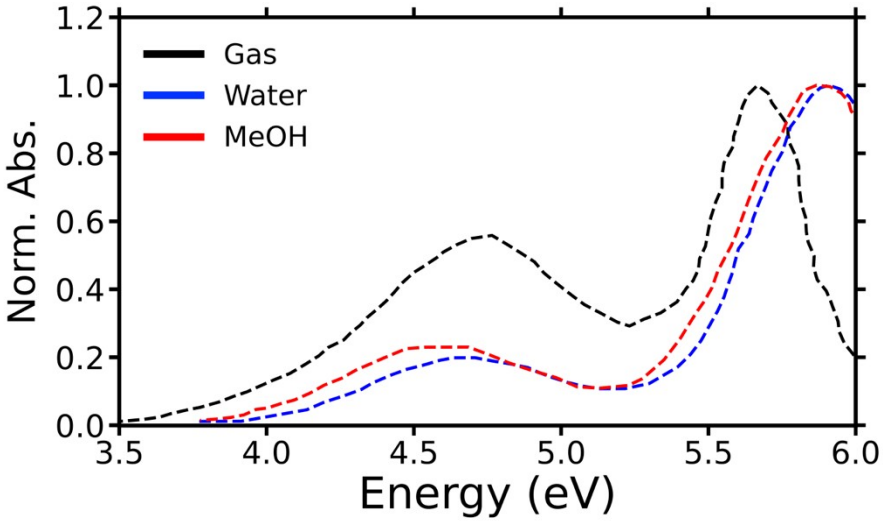

Fig. S17 Normalized experimental absorption spectra of HgI_2 measured in the gas phase, in water and in MeOH.

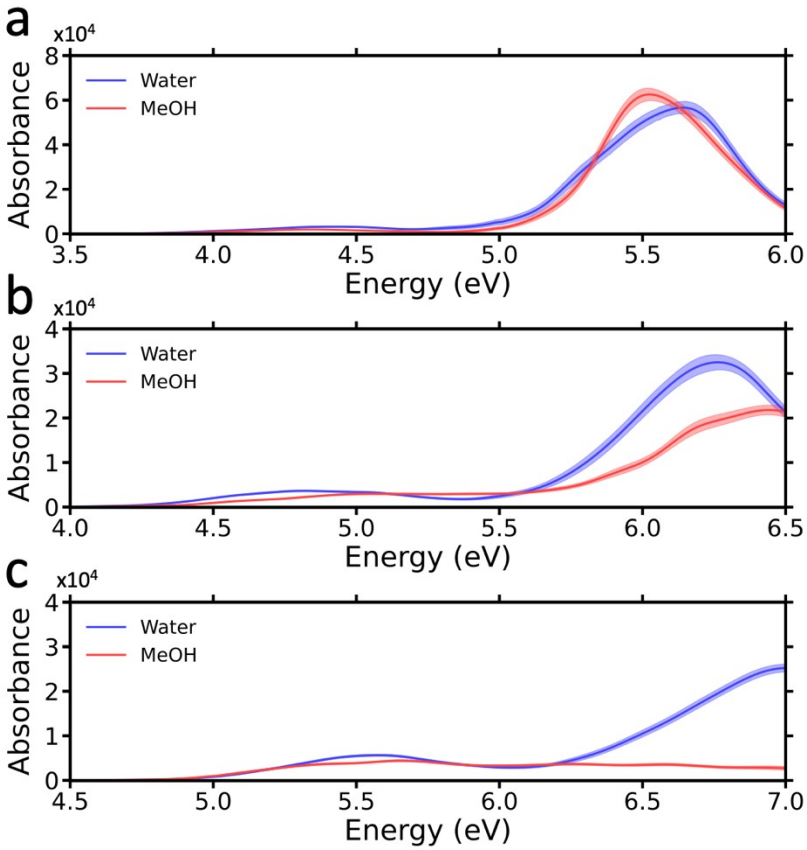

Fig. S18 Calculated absorption spectra and standard deviations of (a) HgI_2, (b) $HgBr_2$, and (c) $HgCl_2$ in water (blue) and MeOH (red), obtained from nuclear ensemble averaging (NEA) approach. Shaded areas indicate the spectral standard deviations, reflecting ensemble-based uncertainty.

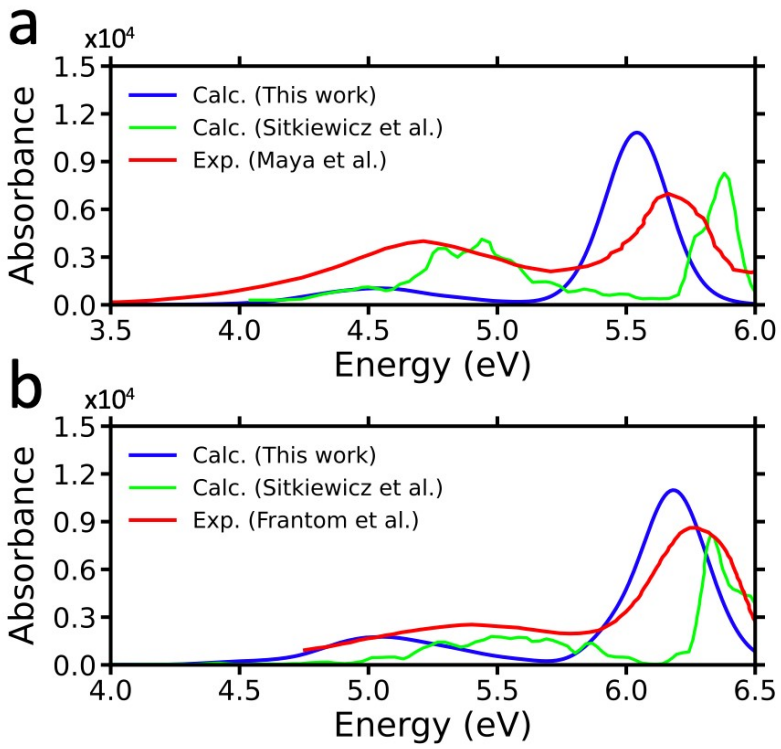

Fig. S19 Comparison of calculated[S2] and experimental gas-phase absorption spectra[S3,S4] of (a) HgI_2 and (b) $HgBr_2$. We note that works of Sitkiewicz et al. employed the CASPT2/PCM level of theory.

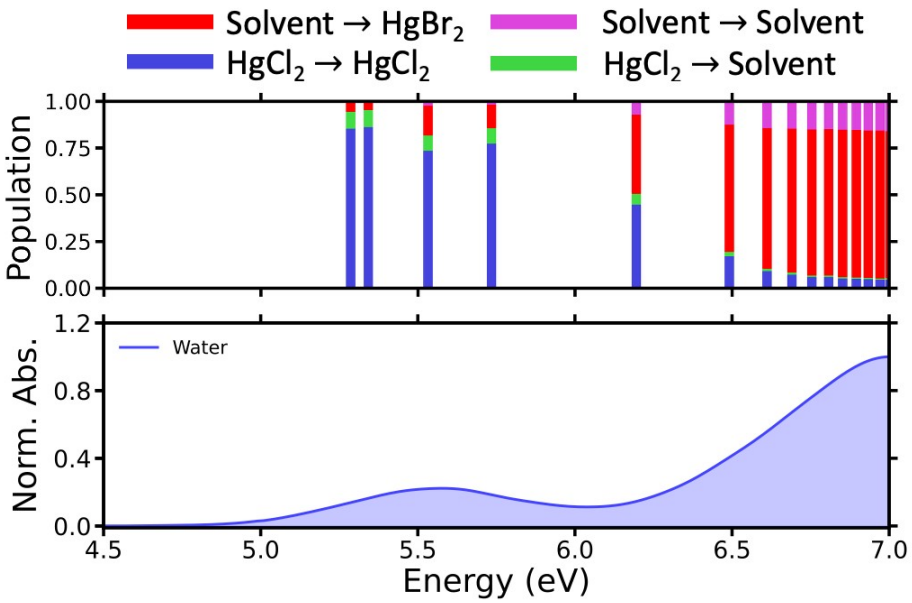

Fig. S20 One-electron transition density matrix (1-TDM) analysis of $HgCl_2$ in water. The systems were partitioned into two fragments: solute and solvent, and the fractional excitation character between these fragments was quantified.

Table S1 Average Mulliken charges of HgX_2 calculated from AIMD snapshots in various solvent environments. The charges of Hg and X atoms are shown in parentheses. For the X atoms, the charges of the two atoms were averaged

	Water	MeOH	DMSO	Pyridine	Gas
HgI_2	-0.60 (0.03, -0.33)	-0.38 (0.16, -0.27)	-0.42 (0.27, -0.35)	-0.43 (0.33, -0.38)	0.00 (0.88, -0.44)
$HgBr_2$	-0.65 (0.18, -0.41)	-0.44 (0.33, -0.39)	–	–	0.00 (0.94, -0.47)
$HgCl_2$	-0.60 (0.27, -0.44)	-0.38 (0.42, -0.40)	–	–	0.00 (1.02, -0.51)

Table S2 Hg–X distance of HgX_2^- molecules, calculated with PBE-D3/def2-TZVPP level of theory

	HgI_2^-	$HgBr_2^-$	$HgCl_2^-$
r(Hg–X) (Å)	3.007	2.813	2.660

Table S3 Excitation energies, oscillator strengths, and electronic transition characters of gas-phase HgI_2, computed at the XMS-CASPT2/ANO-RCC-VTZP level of theory. Electronic states are labeled using the spin–orbit-free (SF) notation

	Energy (eV)	Oscillator strength (f)	Transition character
T_1	3.62	-	5p (I) + 5d (Hg) → Hg–I σ^*
T_2	3.62	-	5p (I) + 5d (Hg) → Hg–I σ^*
S_1	3.86	-	5p (I) + 5d (Hg) → Hg–I σ^*
S_2	3.86	-	5p (I) + 5d (Hg) → Hg–I σ^*
T_3	4.07	-	5p (I) → Hg–I σ^*
T_4	4.07	-	5p (I) → Hg–I σ^*
T_5	4.27	-	Hg–I σ → Hg–I σ^*
S_3	4.30	7.10×10^{-3}	5p (I) → Hg–I σ^*
S_4	4.30	7.10×10^{-3}	5p (I) → Hg–I σ^*
S_5	5.50	6.18×10^{-3}	5p (I) → 6p (Hg) Hg–I σ → Hg–I σ^*

Table S4 The character of spin–orbit coupled (SO) states, oscillator strengths, and electronic transition characters of gas-phase HgI_2, computed at the SO-RASSI/XMS-CASPT2/ANO-RCC-VTZP level of theory

	State character	Energy (eV)	Oscillator strength (*f*)
State 1	S_0 98.7 %	0.00	-
State 2	T_1 49.8 % + T_2 49.8 %	3.36	-
State 3	T_1 49.8 % + T_2 49.8 %	3.36	-
State 4	T_1 67.8 % + S_1 27.8 %	3.46	-
State 5	T_2 67.8 % + S_2 27.8 %	3.46	-
State 6	T_3 49.6 % + T_4 49.6 %	3.82	-
State 7	T_3 49.6 % + T_4 49.6 %	3.82	-
State 8	T_3 74.0 % + S_3 14.8 %	3.89	1.06×10^{-3}
State 9	T_4 74.0 % + S_4 14.8 %	3.89	1.06×10^{-3}
State 10	T_2 49.9 % + T_1 49.9 %	3.96	-
State 11	T_5 53.8 % + T_4 22.8 % + T_3 22.8 %	3.99	-
State 12	T_2 49.4 % + T_1 49.4 %	4.02	-
State 13	T_5 56.3 % + S_3 43.0 %	4.07	2.39×10^{-3}
State 14	T_5 56.3 % + S_4 43.0 %	4.07	2.39×10^{-3}
State 15	S_1 57.4 % + T_1 30.6 %	4.10	-
State 16	S_2 57.4 % + T_2 30.6 %	4.10	-
State 17	T_4 49.3 % + T_3 49.3 %	4.38	5.48×10^{-3}
State 18	T_5 46.1 % + T_4 26.1 % + T_3 26.1 %	4.69	-
State 19	S_1 41.6 % + T_5 35.6 % + T_3 20.6 %	4.78	3.44×10^{-3}
State 20	S_2 41.6 % + T_5 35.6 % + T_4 20.6 %	4.78	3.44×10^{-3}
State 21	T_6 62.1 % + T_{10} 36.1 %	5.19	1.21×10^{-5}
State 22	T_6 62.1 % + T_{10} 36.1 %	5.19	1.21×10^{-5}
State 23	T_8 53.0 % + S_6 46.1 %	5.24	-
State 24	T_7 53.0 % + S_7 46.1 %	5.24	-
State 25	S_5 98.1 %	5.56	7.70×10^{-3}

Table S5 Excitation energies and oscillator strengths of gas-phase HgI_2, calculated at the CAM-B3LYP-D3/X2C-TZVPall level of theory

	Energy (eV)	Oscillator strength (f)
T_1	3.72	-
T_2	3.72	-
S_1	4.13	-
S_2	4.13	-
T_3	4.19	-
T_4	4.19	-
T_5	4.59	-
S_3	4.63	1.16×10^{-2}
S_4	4.63	1.16×10^{-2}
S_5	5.64	8.69×10^{-2}

Table S6 Excitation energy, oscillator strength and electronic transition character of gas-phase $HgBr_2$, calculated with XMS-CASPT2/ANO-RCC-VTZP level of theory. Electronic states are labeled using the SF notation

	Energy (eV)	Oscillator strength (f)	Transition character
T_1	4.23	-	4p (Br) + 5d (Hg) → Hg–Br σ*
T_2	4.23	-	4p (Br) + 5d (Hg) → Hg–Br σ*
S_1	4.51	-	4p (Br) + 5d (Hg) → Hg–Br σ*
S_2	4.51	-	4p (Br) + 5d (Hg) → Hg–Br σ*
T_3	4.81	-	4p (Br) → Hg–Br σ*
T_4	4.81	-	4p (Br) → Hg–Br σ*
T_5	5.00	-	Hg–Br σ → Hg–Br σ*
S_3	5.09	1.50×10^{-2}	4p (Br) → Hg–Br σ*
S_4	5.09	1.50×10^{-2}	4p (Br) → Hg–Br σ*
S_5	6.16	2.22×10^{-3}	4p (Br) → 6p (Hg) Hg–Br σ → Hg–Br σ*

Table S7 The character of spin–orbit coupled (SO) states, oscillator strengths, and electronic transition characters of gas-phase HgI_2, computed at the SO-RASSI/XMS-CASPT2/ANO-RCC-VTZP level of theory

	State character	Energy (eV)	Oscillator strength (f)
State 1	S_0 98.7 %	0.00	-
State 2	T_1 49.8 % + T_2 49.8 %	4.08	-
State 3	T_1 49.8 % + T_2 49.8 %	4.08	-
State 4	T_1 63.9 % + T_2 20.0 %	4.17	-
State 5	T_1 63.9 % + T_2 20.0 %	4.17	-
State 6	T_1 50.0 % + T_2 50.0 %	4.39	-
State 7	T_1 49.9 % + T_2 49.9 %	4.40	-
State 8	S_2 77.4 % + T_1 16.0 %	4.58	-
State 9	S_1 77.4 % + T_1 16.0 %	4.58	-
State 10	T_3 49.6 % + T_4 49.6 %	4.66	-
State 11	T_3 49.6 % + T_4 49.6 %	4.66	-
State 12	T_3 83.6 % + S_4 6.5 %	4.73	1.52×10^{-3}
State 13	T_4 83.6 % + S_3 6.5 %	4.73	1.52×10^{-3}
State 14	T_5 38.2 % + T_4 30.6 % + T_3 30.6 %	4.84	-
State 15	T_5 38.2 % + S_3 28.4 %	4.95	3.87×10^{-3}
State 16	T_5 38.2 % + S_4 28.4 %	4.95	3.87×10^{-3}
State 17	T_4 49.9 % + T_3 49.9 %	4.96	8.96×10^{-4}
State 18	T_5 61.8 % + T_4 18.8 % + T_3 18.8 %	5.11	-
State 19	S_3 59.8 % + T_5 25.1 % + T_4 9.2 %	5.23	9.30×10^{-3}
State 20	S_4 59.8 % + T_5 25.1 % + T_4 9.2 %	5.23	9.30×10^{-3}
State 21	T_6 67.4 % + T_{10} 31.6 %	5.91	7.40×10^{-5}
State 22	T_6 67.4 % + T_{10} 31.6 %	5.91	7.40×10^{-5}
State 23	T_8 52.6 % + S_6 42.1 %	5.98	-
State 24	T_7 52.6 % + S_7 42.1 %	5.98	-
State 25	S_5 95.0 %	6.15	2.08×10^{-3}

Table S8 Excitation energies and oscillator strengths of gas-phase $HgBr_2$, calculated at the CAM-B3LYP-D3/X2C-TZVPall level of theory

	Energy (eV)	Oscillator strength (f)
T_1	4.25	-
T_2	4.25	-
S_1	4.69	-
S_2	4.69	-
T_3	4.84	-
T_4	4.84	-
T_5	5.27	-
S_3	5.31	2.22×10^{-2}
S_4	5.31	2.22×10^{-2}
S_5	6.34	8.14×10^{-2}

Table S9 Excitation energy, oscillator strength and electronic transition character of gas-phase $HgCl_2$, calculated with XMS-CASPT2/ANO-RCC-VTZP level of theory. Electronic states are labeled using the SF notation

	Energy (eV)	Oscillator strength (f)	Transition character
T_1	4.83	-	3p (Cl) + 5d (Hg) → Hg–Cl σ^*
T_2	4.83	-	3p (Cl) + 5d (Hg) → Hg–Cl σ^*
S_1	5.13	-	3p (Cl) + 5d (Hg) → Hg–Cl σ^*
S_2	5.13	-	3p (Cl) + 5d (Hg) → Hg–Cl σ^*
T_3	5.53	-	3p (Cl) → Hg–Cl σ^*
T_4	5.53	-	3p (Cl) → Hg–Cl σ^*
T_5	5.73	-	Hg–Cl σ → Hg–Cl σ^*
S_3	5.85	1.80×10^{-2}	3p (Cl) → Hg–Br σ^*
S_4	5.85	1.80×10^{-2}	3p (Cl) → Hg–Br σ^*
S_5	6.78	6.80×10^{-3}	3p (Cl) → 6p (Hg) Hg–Cl σ → Hg–Cl σ^*

Table S10 The character of spin–orbit coupled (SO) states, oscillator strengths, and electronic transition characters of gas-phase $HgCl_2$, computed at the SO-RASSI/XMS-CASPT2/ANO-RCC-VTZP level of theory

	State character	Energy (eV)	Oscillator strength (f)
State 1	S_0 98.7 %	0.00	-
State 2	T_1 49.9 % + T_2 49.9 %	4.78	-
State 3	T_1 49.9 % + T_2 49.9 %	4.78	-
State 4	T_1 71.0 % + T_2 26.7 %	4.82	-
State 5	T_2 71.0 % + T_1 26.7 %	4.82	-
State 6	T_1 49.9 % + T_2 49.9 %	4.88	-
State 7	T_1 50.0 % + T_2 50.0 %	4.88	-
State 8	S_1 97.7 %	5.14	-
State 9	S_2 97.7 %	5.14	-
State 10	T_3 49.6 % + T_4 49.6 %	5.47	-
State 11	T_3 49.6 % + T_4 49.6 %	5.47	-
State 12	T_3 95.5 %	5.51	3.72×10^{-4}
State 13	T_4 95.5 %	5.51	3.72×10^{-4}
State 14	T_4 47.9 % + T_3 47.9 %	5.56	-
State 15	T_4 49.6 % + T_3 49.6 %	5.57	-
State 16	T_5 94.3 %	5.73	9.32×10^{-4}
State 17	T_5 94.3 %	5.73	9.32×10^{-4}
State 18	T_5 96.5 %	5.74	-
State 19	S_3 86.5 % + S_4 5.0 %	5.86	1.66×10^{-2}
State 20	S_4 86.5 % + S_3 5.0 %	5.86	1.66×10^{-2}
State 21	T_6 73.4 % + T_{10} 25.7 %	6.57	9.69×10^{-5}
State 22	T_6 73.4 % + T_{10} 25.7 %	6.57	9.69×10^{-5}
State 23	T_6 82.7 % + S_8 16.5 %	6.65	-
State 24	T_8 56.4 % + S_6 41.0 %	6.66	-
State 25	T_9 56.4 % + S_7 41.0 %	6.66	-
State 26	T_8 49.6 % + T_9 49.6 %	6.72	6.11×10^{-5}
State 27	T_8 49.6 % + T_9 49.6 %	6.72	6.11×10^{-5}
State 28	S_5 81.2 % + T_{10} 18.0 %	6.72	5.53×10^{-3}

Table S11 Excitation energies and oscillator strengths of gas-phase $HgCl_2$, calculated at the CAM-B3LYP-D3/X2C-TZVPall level of theory

	Energy (eV)	Oscillator strength (f)
T_1	4.84	-
T_2	4.84	-
S_1	5.33	-
S_2	5.33	-
T_3	5.57	-
T_4	5.57	-
T_5	6.01	-
S_3	6.10	2.37×10^{-2}
S_4	6.10	2.37×10^{-2}
S_5	6.95	4.29×10^{-2}

Supplementary References

(S1) T. R. Griffiths and R. A. Anderson, *J. Chem. Soc., Faraday Trans. 2*, 1979, **75**, 957.

(S2) S. P. Sitkiewicz, D. Rivero, J. M. Oliva-Enrich, A. Saiz-Lopez and D. Roca-Sanjuán, *Phys. Chem. Chem. Phys.*, 2019, **21**, 455–467.

(S3) J. Maya, *J. Chem. Phys.*, 1977, **67**, 4976–4980.

(S4) G. L. Frantom. UV Absorption Cross-Section of Mercury Bromide; Master's Thesis, Air Force Institute of Technology, Air University, Wright-Patterson Air Force Base, United States, 1979.